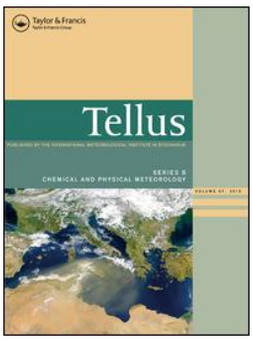

Tellus B: Chemical and Physical Meteorology

ISSN: (Print) 1600-0889 (Online) Journal homepage: http://www.tandfonline.com/loi/zelb20

A modelling study on the activation of small Aitken-mode aerosol particles during CIME 97

Guiléne Gérémy, Wolfram Wobrock, Andrea I. Flossmann, Alfons Schwarzenböck & Stephan Mertes

To cite this article: Guiléne Gérémy, Wolfram Wobrock, Andrea I. Flossmann, Alfons Schwarzenböck & Stephan Mertes (2000) A modelling study on the activation of small Aitken-mode aerosol particles during CIME 97, Tellus B: Chemical and Physical Meteorology, 52:3, 959-979, DOI: 10.3402/tellusb.v52i3.17078

To link to this article: https://doi.org/10.3402/tellusb.v52i3.17078

Tellus (2000), 52B, 959–979
Printed in UK. All rights reserved

TELLUS
ISSN 0280–6509

A modelling study on the activation of small Aitken-mode aerosol particles during CIME 97

By GUILÉNE GÉRÉMY[1], WOLFRAM WOBROCK[1], ANDREA I. FLOSSMANN[1]*, ALFONS SCHWARZENBÖCK[2] and STEPHAN MERTES[2] [1]*Laboratoire de Météorologie Physique, Université Blaise Pascal-CNRS-OPGC, 24, avenue des Landais, F-63177 Aubière Cedex, France;* [2]*Institut für Troposphärenforschung, Permoserstr. 15, D-04303 Leipzig, Germany*

(Manuscript received 18 December 1999; in final form 5 July 1999)

ABSTRACT

During February 1997, one of the 2 observational periods of CIME (*c*loud *i*ce *m*ountain *e*xperiment), a joint field experiment funded by the European Commission, took place on the summit of the Puy de Dôme in the centre of France. During this experiment the droplet spectra were measured with an FSSP and the aerosol particles in the drops and in the interstitial particle phase were measured with a counterflow virtual impactor and a round jet impactor inside a windtunnel. Very low aerosol particle and drop concentrations were observed and particles as small as 25 nm in diameter were found to activate. Two datasets obtained on 15 February and 17 February were used to study the activation of the small Aitken-mode particles and the spectral form of the droplet spectrum and the scavenging fraction. Numerous sensitivity studies were performed investigating the rôle of the number density and chemical composition of the aerosol particles. The rôle of mixing inside the orographic cloud was studied by using a new technique. It considers the fact that the air arriving on the summit of the Puy de Dôme is a mixture of air of different origins. Thus, it weighs the results of a spectral scavenging model (DESCAM or EXMIX) calculated along a number of individual trajectories. The weighing function is derived from tracer and trajectory studies with a 3-dimensional mesoscale model. The model was able to reproduce the activation of aerosol particles as small as 25 nm. It was caused by the low aerosol particle number concentrations. In general, we can conclude that the variability found in the sensitivity tests of the dynamical and chemical factors allows to reproduce the shape of the observed results. As too many free parameters exit at the moment we cannot quantify the contribution of each factor studied to the observed scavenging fraction, however, it seems that dynamics dominates.

1. Introduction

Clouds cover at all times large fractions of our planet. They play a crucial rôle in the hydrological cycle, act as chemical "factories" by scavenging atmospheric trace constituants and are recognised to be an important factor in determining the climate of the earth (ICCP, 1995). Thus, the investigation of clouds is a significant element in our striving to understand the functioning of the atmosphere. One aspect of this investigation are field campaigns trying to study in-situ the clouds, another aspect are numerical simulations which help to generalise the hypotheses. Even though cloud modelling has enormously advanced over the last decades and arrive at successfully predicting cloud dimensions and liquid water content still problems remain unsolved. One, which has been extensively discussed in the literature (Colvile et al., 1994; Wobrock et al., 1994; Hallberg et al.,

* Corresponding author.
e-mail: flossman@opgc.univ-bpclermont.fr

1997) is the problem of modelling the droplet size distribution. Already thirty years ago (Twomey, 1959; Warner, 1969, 1973) this problem has been identified. Noone et al. (1992) have identified a related problem connected to the determination of the "scavenging fraction", i.e., the fraction of the initial aerosol particle spectrum that has served as cloud condensation nuclei (CCN). Since then, the problem has been narrowed down and it has been found that the exact knowledge of the initial aerosol particle size distribution and its chemical nature which supply the CCN is of utmost importance (Hallberg et al., 1994, 1997). In the past years this problem has been addressed in a number of different campaigns. Noone et al. (1992) reported, e.g., for a polluted ground fog near Bologna (Italy) that aerosol particles between 0.4–0.7 μm have activated to form drops. Hallberg et al. (1994) have reported values of 0.08–0.2 μm for the orographic clouds at Kleiner Feldberg, a mountain site in a polluted part of Germany, and Martinsson et al. (1997) have measured values larger than 0.1 μm in the cap clouds of the Great Dun Fell in a less polluted air mass of northern England. In all these cases, the scavenging function showed an S-type shape with a "cut-off" smeared out over several hundred nanometers (see Noone et al.; 1992 for a discussion of the concept).

It seems, however, that the size and the chemical composition of the particles is not the only factor. The complex mixing and entrainment going on in clouds at different level will also mix in fresh CCN. Those will broaden, e.g., the drop spectrum beyond the one predicted only from the theory of simple adiabatic ascent (Warner, 1969, 1973; Baker and Latham, 1979, 1982; Baker et al., 1980) and change the scavenging fraction (Noone et al., 1992). Taking into account the composition and distribution of the aerosol particles and the mixing going on in clouds has improved the modelling of the drop number distribution and the scavenging fraction. However, it is still not possible to exactly reproduce the measured distributions.

In order to further advance in this direction we have employed in the current study a novel approach to simulate the mixing in a cloud forming orographically at a mountain site, thus, complementing and extending our previous study (Hallberg et al., 1997). Then, we have simulated the clouds observed at the summit of the Great Dun Fell mountain in the North of England during the 1993 GCE (Ground based Cloud Experiment) of EUROTRAC (see special issue of *Atmospheric Environment*, vol. 31, no. 16 for description). We have modelled, then, the cloud droplet spectrum and compared it to the measured ones initialising the model with measured aerosol particle size distributions resulting from Differential Mobility Particle Sizer and impactor measurements. We noticed, then, a strong dependency whether we assumed that the air arriving at the summit originated from a surface trajectory or an elevated trajectory (Fig. 2d of Hallberg et al., 1997).

Consequently, in the present study we modified the model and studied the droplet spectra and the scavenging fraction as a function of different trajectories originating at different levels between the surface and the trajectory grazing the summit. Numerical tracer experiments allow to derive weighing functions to define relative contributions of the different levels to the summit air. With this new tool we perform several sensitivity studies concerning the drop spectrum and scavenging fraction.

As a basis we selected the observations performed during the first measuring period (February, 1997) of CIME (*c*loud *i*ce *m*ountain *e*xperiment), a joint field experiment funded by the European Commission in order to study the fate of pollutants during the freezing of a cloud (CIME, 1998). During the first measuring period the objectives of CIME could not be reached, as the temperatures remained too high (above -3°C), thus, a successful second measuring period was appended in February 1998. This will be subject of a separate publication.

However, the instrumentation during the first measuring period allowed to obtain a dataset interesting for the investigation performed in the current paper, as this time the initial aerosol particle size distribution was measured by a CVI (counterflow virtual impactor) (Schwarzenböck, 1998). Also, here, for the first time the activation of small Aitken-mode particles as low as 25 nm was measured while the total number concentration of the particles and drops was quite low (Schwarzenböck et al., 1998). The aim of this paper is to understand the measured drop spectra and scavenging fraction and their sensitivity with respect to a number of parameters including mixing processes.

Section 2 will shortly explain the experimental set-up and the obtained measurements. Sections 3, 4 will present the applied model tools and the initial conditions used for the model simulations. The results and the discussion are presented in Sections 5 and 6.

2. Measurements of the interstitial and residual aerosol particles

2.1. Experimental set-up

The main measuring platform during CIME was the cloud-windtunnel on the Puy de Dôme, an ancient volcano (1465 m) in the centre of France, which was equipped with a great number of microphysical, particle, and gas measuring instruments. For this modelling study we will only exploit the observations of droplet spectra, and the spectra of interstitial and residual aerosol particles obtained on 15 and 17 February 1997.

The meteorological conditions for both events differed strongly. On 15 February a cold front passed the observational site, northerly wind conditions and temperature between -4 and -3°C prevailed. The observations presented here were taken in the final phase of the cloud presence where strong mixing processes prevailed.

The measurements taken on the afternoon of 17 February 1997 respresent more typically the capped cloud condition on Puy de Dôme. Then, westerly winds prevailed which forced the ascent of humid air in a stably stratified boundary layer leading to the formation of the characteristic "chapeau" on the PDD. Temperature was around 0°C, wind speeds on the summit 10–12 m/s.

The droplet spectra were measured by a PMS FSSP-100, which was installed outside the windtunnel. When the instrument was exposed to the supercooled air it rapidly iced. Thus, only directly after de-icing the measurements can be considered as free of artefacts. Consequently, only few reliable measurements of the droplet spectra are available.

The interstitial and residual aerosol particles were measured inside the cloud-windtunnel under controlled conditions. The inlet used to sample cloud droplets was a Counterflow Virtual Impactor (CVI, Ogren et al., 1985) which was developed for the CIME campaign by the Institut für Troposphärenforschung, Leipzig (Schwarzenböck, 1998). With the CVI, hydrometeors larger than the cut size of the probe (5 μm in diameter) are impacted from the ambient air into a dry and particle-free carrier airstream. Once sampled, each droplet is evaporated leaving behind a residual particle while water and other volatile species in the hydrometeors are driven into the gas phase. A Differential Mobility Particle Sizer (DMPS) and a Lyman-α hygrometer allow the characterisation of the residual aerosol particles and their initial liquid water content. The outer housing of the CVI was heated with heating foils underneath to prevent icing of the CVI in its high speed wind tunnel. The heating foils were neither in contact with the CVI sample flow tubing nor with the sample flow itself to exclude artefacts (see CIME, 1999).

Hydrometeors and non-activated interstitial particles smaller than 5 μm in diameter were sampled by using a Round Jet Impactor (RJI) installed next to the CVI in the windtunnel (Schwarzenböck, 1998), dried on the way to the second DMPS system in order to observe the size distribution of the interstitial particle spectrum.

The collection efficiency curves of the CVI and the RJI are presented in Schwarzenböck et al. (1997) and CIME (1999). The calibrated sampling efficiency for the CVI increases from 15% to 85% (5% to 95%, respectively) within a size range of the aerodynamic cloud element diameter of less than 2 μm (4 μm, respectively). The CVI contamination with smaller particles can, thus, be considered non-significant. Analogous results were obtained for the calibration of the RJI (CIME, 1998). Considering the cut-size of 5 μm in diameter we can, however, not exclude that unactivated aerosol particles larger than this size were measured by the CVI and that activated drops existing below this size were sampled by the RJI. This is supported by the fact that on 17 February the FSSP reported at 204 drops per cm^3 while the CVI recorded only 128 residual particles cm^{-3} (15 February at 11:00: 221 cm^{-3} FSSP versus 210 cm^{-3} CVI). Thus, when we talk about interstitial or residual particles these terms apply to the 2 reservoirs measured by CVI and RJI. Also the model results presented later take into account these limitations.

2.2. Observational results for the scavenging fraction

The sampling approach with 2 identical DMPS for CVI and RJI allows a direct comparison of

particles within the same dry particle size range, which did and did not grow larger than 5 μm. The fraction of the total number of aerosol particles within one size bin that is found in cloud droplets is defined as

$$F_{Ni} = \frac{N_{i,\mathrm{CVI}}}{N_{i,\mathrm{CVI}} + N_{i,\mathrm{RJI}}}, \quad (1)$$

where $N_{i,\mathrm{CVI}}$ is the number concentration for the size bin i measured with the CVI inlet, and $N_{i,\mathrm{RJI}}$ is the number concentration in the same size bin i measured with the interstitial (i.e., round jet impactor) inlet. F_{Ni} is also called *the scavening fraction.*

In Figs. 1a,b we present 2 measurements of the dry particle size distribution obtained by the DMPS units behind the interstitial and the CVI inlet and the derived scavenging fraction. The measurements were obtained in clouds on 15 and 17 February 1997. Both results represent averages

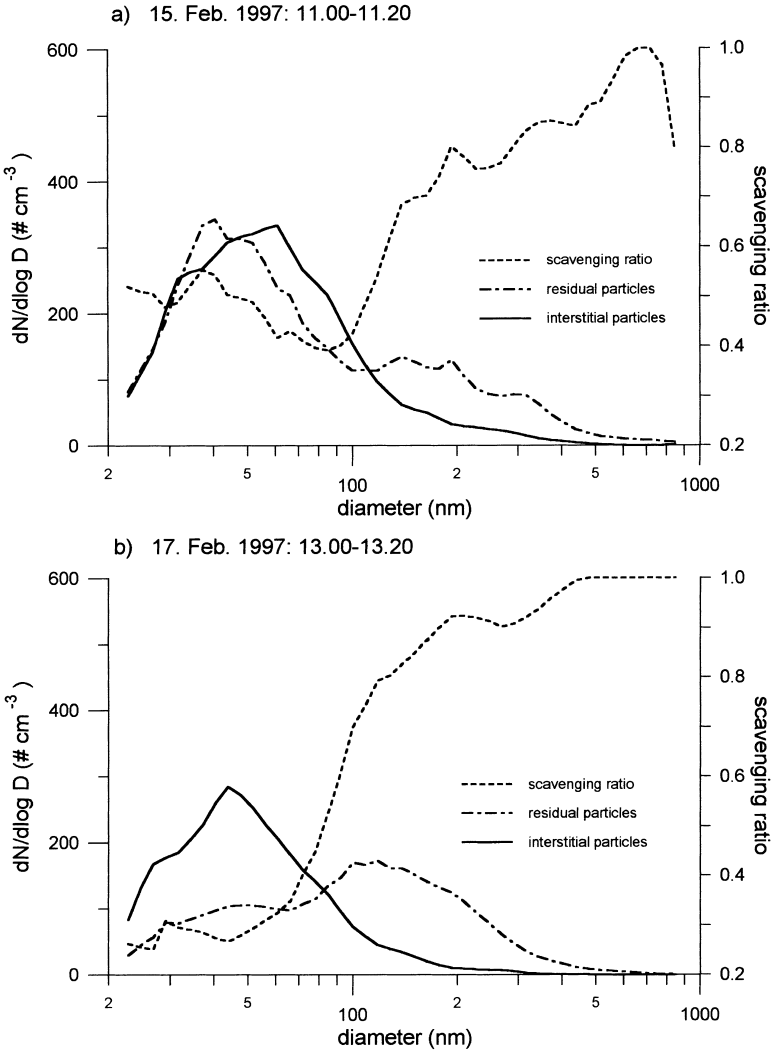

Fig. 1. Measurements of the number of interstitial aerosol particles by the RJI (solid line), the number of residual aerosol particles by the CVI (dotted line) and the resulting scavenging fraction calculated from eq. (1) for (a) 15 February 1997 and (b) 17 February 1997.

over 20 min. The error in these measurements range from 10% for the small particles to about 20% for the large.

3. Model description

The model results presented here make use of 3 different modules. The first one is a dynamic module, which is a 3-D mesoscale model. Embedded into trajectories calculated by the 3-D model, a 0-D lagrangian parcel model is launched which includes a spectral microphysical cloud model. Here, we employed 2 different modules. We will first present the 3-D dynamic model, then the 2 modules for microphysics and scavenging and then their coupling with the dynamic framework.

3.1. *The 3-D dynamic mesoscale model of Clark and Hall*

The dynamic framework employed in the present study is the 3-dimensional model developed by Clark and co-workers (Clark, 1977, 1979; Clark and Gall, 1982; Clark and Farley, 1984; Hall, 1980). This model is an established tool for the simulation of the air flow and the formation of clouds over complex terrain on small meteorological scales (Clark et al., 1994; Bruintjes et al., 1995; Wobrock et al., 1997). The present non-hydrostatic version of the code uses a terrain following vertical co-ordinate with a user-defined spacing. The bulk cloud liquid water is determined by a saturation adjustment, as described in Bruintjes et al. (1995).

3.2. *The microphysics module DESCAM*

One of the microphysics employed in the present study is the module DESCAM, i.e., the *de*tailed *sca*venging and *m*icrophysical model as discussed in Flossmann et al. (1985, 1987) coupled to a 0-D Lagrangian parcel model dynamics. There, the aerosol particles are treated by a spectral number or mass density distribution function $\psi(m_{AP})$ with m_{AP} being the radius of the moist aerosol particle:

$$\frac{\partial\psi(m_{AP})}{\partial t} = -\mu[\psi(m_{AP}) - \psi'(m_{AP})]U + \left.\frac{\partial\psi(m_{AP})}{\partial t}\right|_{act} + \left.\frac{\partial\psi(m_{AP})}{\partial t}\right|_{con/eva} + \left.\frac{\partial\psi(m_{AP})}{\partial t}\right|_{imp} \quad (2)$$

Apart from dynamical, i.e., entrainment processes considered by the first term on the right-hand side of eq. (2) (μ is the entrainment parameter, U the vertical velocity of the air parcel, and the primed values pertain to the values in the unperturbed environment), the number of particles of a certain size changes due to activation to drops (act), due to size changes resulting from humidity changes (con/eva), and due to impaction scavenging by drops (imp). The nucleated drops are also described by a spectral number or mass density distribution function $\psi(m)$ with m being the radius of the drop.

$$\frac{\partial\psi(m)}{\partial t} = -\mu[\psi(m)]U + \left.\frac{\partial\psi(m)}{\partial t}\right|_{act} + \left.\frac{\partial\psi(m)}{\partial t}\right|_{con/eva} + \left.\frac{\partial\psi(m)}{\partial t}\right|_{imp} + \left.\frac{\partial\psi(m)}{\partial t}\right|_{coll/coal} + \left.\frac{\partial\psi(m)}{\partial t}\right|_{break}. \quad (3)$$

They grow by condensation or evaporate (con/eva), collide and coalesce (coll/eva), and eventually break up. During their lifetime they further scavenge particles (imp) and the scavenged pollutant mass is redistributed through the microphysical processes. The extension of this microphysical and scavenging model to the scavenging of 2 different types of aerosol particles (e.g., $(NH_4)_2SO_4$ and NaCl for marine air masses) is described in Flossmann (1991) and the inclusion of effects of gaseous H_2O_2 and O_3 on the uptake and oxidation of SO_2 was presented in Flossmann (1994). The version used here contains prognostic equations for 4 distribution functions ψ as summarised in Table 1. For further details on the terms changing the density distribution functions see Flossmann et al. (1985) and Flossmann (1994). The resulting droplet spectra are compared with the measurements of the FSSP.

As the model was designed to simulate the full droplet spectrum up to raindrop sizes, the scavenged aerosol particle, e.g., is lumped together in one mass density distribution function ψ disregarding the fact that in one droplet category m we may find small as well as large particles. Thus, when evaporating the droplet spectrum the detailed information on the initial aerosol particle spectrum can only partly be retrieved (Hatzianastassiou et al., 1998). In order to remedy

Table 1. *Four density distribution functions as used in the DESCAM model with m being the drop mass and m_{AP} being the aerosol particle mass; the drop and aerosol particle categories are logarithmically equally spaced with a mass doubling every second category*

Density distribution function		No. of classes, minimum and maximum radius
f_d (m)	drop number density distribution function	69, 1 μm–2580 μm
g_{APd} (m)	mass density distribution function for particles in the drops	69, 1 μm–2580 μm
f_{APa} (m_{AP})	aerosol particle number density distribution function for particles in the air	81, 10^{-3} μm–10 μm
g_{APa} (m_{AP})	the mass density distribution function for particles in the air	81, 10^{-3} μm–10 μm

this problem we have also used a second microphysical module: the model EXMIX.

3.3. *The microphysics module EXMIX*

The model EXMIX was developed by Wobrock (1986) in order to study the growth of *ex*ternally *mix*ed condensation nuclei in fog and clouds. It allows at all times to follow the individual activated aerosol particles through the droplet spectrum as it considers only one number density distribution function $\psi = f$ for all aerosol particles and droplets together. The information on the aerosol nucleus and the attached water mass are followed via 2 coordinates m for the droplet mass and $m_{AP,N}$ for the mass of the dry aerosol nucleus. In order to take into account the externally mixed aerosol a third coordinate x_i for the chemical composition is considered with

$$x_i = x_i(\varepsilon_s, \rho_n, M_s, v_s), \quad i = 1, \ldots, n.$$

Herein, n types of condensation nuclei can be distinguished differing in solubility fraction ε_s, density of aerosol particles ρ_n, molecular weight M_s, and number of free ions v_s. Thus, the time rate of change of $\psi = f$ is:

$$\frac{\partial f(m, m_{AP,N}, x_i)}{\partial t} = -\mu[f(m, m_{AP,N}, x_i) - f'(m, m_{AP,N}, x_i)]U - \frac{\partial}{\partial m}\left[f(m, m_{AP,N}, x_i)\frac{dm}{dt}\right], \quad (4)$$

where dm/dt represents the droplet growth equation as described in Pruppacher and Klett (1997):

$$\frac{dm}{dt} = 4\pi r \frac{\frac{e}{e_{sat,w}} - \exp(Y)}{\frac{\rho_w R^* T}{e_{sat,w} D'_v M_w} + \frac{L_e \rho_w}{k'_a T}\left(\frac{L_e M_w}{TR^*} - 1\right)}, \quad (5)$$

$$Y = \frac{2\sigma_s}{\rho_w R_v T a} - \frac{\varepsilon_s M_s \rho_n r^3 \phi v_s}{M_s \rho_w (a^3 - r^3)}, \quad (6)$$

with e: actual water vapour pressure; $e_{sat,w}$: saturation vapour pressure; M_w: molecular weight of water; ϕ: osmotic coefficient of salt in solution; a: radius of moist aerosol particle or drop; r: radius of the dry aerosol fraction of insoluble material in the aerosol nucleus; ρ_w: density of water; R^*: universal gas constant; R_v: gas constant of water vapour; σ_s: surface tension; L_e: latent heat of evaporation. The right-hand side of eq. (4) corresponds to the first and third term on the right-hand side of eq. (3). D'_v: modified diffusion coefficient and k'_a: modified thermal conductivity (Pruppacher and Klett, 1997) read:

$$D'_v = \frac{D_v}{\frac{a}{a + \Delta_v} + \frac{D_v}{a\alpha_c}\left(\frac{2\pi M_w}{R^* T}\right)^{1/2}}, \qquad k'_a = \frac{k_a}{\frac{a}{a + \Delta_T} + \frac{k_a}{a\alpha_T \rho c_p}\left(\frac{2\pi M_a}{R^* T}\right)^{1/2}} \quad (7)$$

herein, Δ_v: vapour jump length; Δ_T: thermal jump distance; α_c: condensation coefficient; α_T: thermal accommodation coefficient. These values were

taken as suggested by Pruppacher and Klett (1997).

The advantage of EXMIX is that we can attribute to each aerosol particle a different chemistry and its growth by condensation to form a drop, and later its evaporation is correctly calculated. Furthermore, it does not need an activation term as aerosol particles and drops are treated in the same number density distribution function. This means that also the transition from sub- to supersaturation and vice versa can be described continuously as long as we stay above the deliquescence point of the particles. Comparison of EXMIX simulations with results of field experiments can be found in Schell et al. (1997) and Laj et al. (1997).

The disadvantage of this model is that it only considers the diffusional growth process and entrainment but no collision/coalescence, break up and impaction scavenging. However, estimates with the DESCAM model confirmed that the collision and coalescence process as well as break up and impaction scavenging are negligible in the considered orographic cloud (see also Hallberg et al. (1997)).

In order to be able to compare the output of EXMIX as realistically as possible with the measurements of CVI and RJI the *modelled spectrum has been multiplied with the collection efficiency curves of CVI and RJI* (Scharzenböck et al., 1997; CIME, 1999) before calculating the scavenging fraction.

3.4. *The microphysical modules in the 3-D framework*

The dynamic model calculates for the simulation period the complete 3-dimensional field of temperature, humidity, liquid water content and the 3 wind components. Thus, it allows to calculate trajectories or back-trajectories starting at different points. Each point along the trajectories is characterised by a complete set of dynamic and thermodynamic variables, which are used to drive the 0-D parcel model.

The DESCAM as well as the EXMIX model need as a starting value temperature, dew points and the vertical wind speed near cloud base. Along the in-cloud trajectory temperature changes by:

$$\frac{\mathrm{d}T}{\mathrm{d}t} = -\frac{gU}{c_\mathrm{p}} - \mu(T - T')U + \frac{L_\mathrm{e}}{c_\mathrm{p}} C_\mathrm{ph}. \tag{8}$$

The first term on the right-hand side represent the adiabatic ascent with g acceleration of gravity, and c_p specific heat at constant pressure. The second term represent the entrainment where T' is the temperature outside the air parcel. The third 3rd treats the heat set free by condensation with L_e latent heat of condensation and C_ph is the rate of phase change calculated by DESCAM or EXMIX microphysics.

The vertical wind speed U is taken from the trajectory values. The entrainment parameter μ is calculated from:

$$\mu = \frac{\alpha}{R}, \tag{9}$$

with $\alpha = 0.6$ and R radius of the air parcel calculated from:

$$\frac{\mathrm{d}\ln R}{\mathrm{d}t} = \frac{1}{3}\left(\mu U - \frac{\mathrm{d}\ln \rho}{\mathrm{d}t}\right), \tag{10}$$

as detailed in Flossmann et al. (1985). Here, ρ density of air.

For the cases where no entrainment was considered μ was set to zero. In the cases where a trajectory *ensemble* was calculated the microphysical values at the Puy de Dôme summit were derived by weighing the results ψ_i of the individual trajectory calculations by:

$$\psi = \sum_i \psi_i \varepsilon_i,$$

where ε_i are the weight functions for the different trajectories as explained in Subsection 5.1.

4. Initial conditions

4.1. *Initialisation of the dynamic Clark model*

For the simulation we chose a domain of $25 \cdot 22\ \mathrm{km}^2$ with a grid increment of $\Delta x = \Delta y = 0.2$ km centred around the Puy de Dôme. Fig. 2 displays the location of the Puy de Dôme within France and the topography of the region.

We selected 2 different meteorological situations for our study. The first occurred on 15 February 1997. At 12.00 UTC France was located between 2 fronts: the first was oriented south-west/north-east and located over the southern part of France. The second was a cold front over the northern Atlantic Ocean. The observations at the top of the Puy de Dôme indicated a temperature decrease

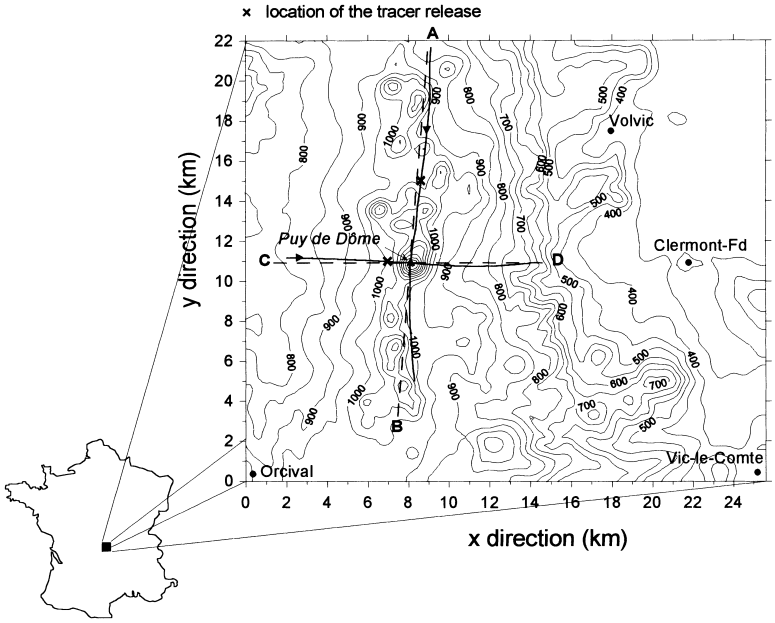

Fig. 2. Map of the location of the Puy de Dôme within France and the topography of the region considered. For 15 (17) February 1997 the solid curve along AB (CD) gives the path of the air touching the summit. The dashed curves indicate the cross-sections used for Fig. 4. The crosses indicate the position of the columns launching tracers for the 15 and 17 February.

of 3°C between 8.30 and 10.00 UTC, sign of the cold front crossing the site. The synoptic influence dominated. Cloud formation occurred between 8.30 and 11.00 UTC at the top of the Puy de Dôme. The LWC was around 0.4–0.5 g m^{-3}. The clouds began to dissipate at 11.30 and the LWC decreased to about 0.15 g m^{-3}. During the period between 10.00 and 14.00 northerly winds prevailed at the measuring site (7–10 m s^{-1}).

A complementary situation occurred on 17 February 1997. At 12.00 UTC the northern part of France was under the influence of a succession of atmospheric depressions centred on the north-west of Great Britain, however, the fronts did not pass the observational site. The temperature stayed almost constant around 0°C. An orographic cloud was observed on the top of the Puy de Dôme with LWCs around 0.3 g m^{-3}. The cloud had dissipated around 16.30 UTC. During the period between 10.00 and 14.00 westerly winds were observed on the summit of the Puy de Dôme.

The model was initialised with the soundings observed at 11:00 UTC at Lyon for the 15 February and at Bordeaux for the 17 February 1997. We studied the situation in both cases after 2.5 h of model time when the clouds were well developed.

4.2. *Initialisation of the microphysical models DESCAM and EXMIX*

The initial values for temperature, humidity and wind were those calculated by the 3-D model. The initial dry aerosol particle spectrum was derived by a numerical fit to the observed aerosol particle distribution measured by the CVI and the RJI on the summit of the Puy de Dôme (Fig. 1). For the numerical fit we used a superposition of 3 lognormal distributions as proposed by Jaenicke (1988):

$$\frac{\mathrm{d}N}{\mathrm{d}\ln r} = f_{\mathrm{APa}}(\ln r) = \sum_{i=1}^{3} \frac{n_i}{(2\pi)^{1/2}\log\sigma_i \ln 10} \times \exp\left(-\frac{[\log(r/R_i)]^2}{2(\log\sigma_i)^2}\right). \quad (11)$$

The number density distribution function resulting from the measurements (Fig. 1) and the numerical

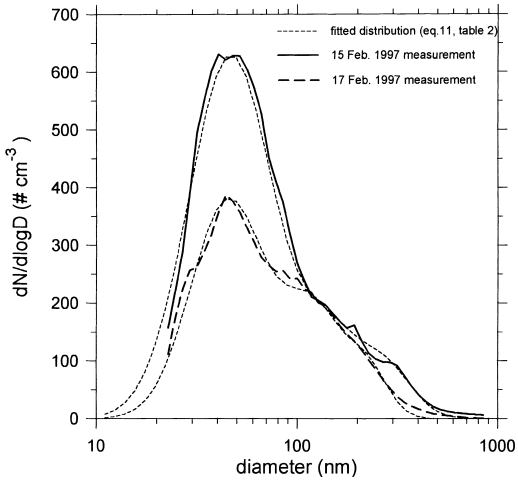

Fig. 3. Measured number density distribution functions for aerosol particles for the 15 February 1997 (solid curve) and 17 February 1997 (dashed curve). The dotted curves give the number density distribution function of aerosol particles resulting from eq. (11) and Table 2.

fits are displayed in Fig. 3. They are summarised in Table 2. During this period of the CIME campaign no measurements concerning the chemical composition of the particles were made. Thus, for the DESCAM simulations it was assumed that all particles consisted of 50% $(NH_4)_2SO_4$ and 50% insoluble material. With the EXMIX model, however, several sensitivity tests were performed varying the chemical composition of the particles as well as their solubility. The different cases considered with EXMIX are summarised later in Tables 4–6.

Table 2. *Parameters for the aerosol particle distribution as used in the DESCAM and EXMIX model for the air parcel dynamics; n_i = total number of aerosol particles per cm^3; R_i = geometric mean aerosol particle radius in μm; σ_i = standard deviation in mode i; chemical composition of the aerosol particle modes*

	15 February 1997			17 February 1997		
Mode i	n_i	R_i	log σ_i	n_i	R_i	log σ_i
1	760	0.0233	0.21	400	0.0225	0.184
2	119	0.073	0.15	164	0.0606	0.153
3	61	0.14	0.129	40	0.114	0.098

5. Results

5.1. *Results of the dynamic calculations with the 3-D model*

On 15 February, a northerly flow prevailed. As this flow is in the line of the chain of the mountains the air arriving at the summit of the Puy de Dôme had already lived various ascents and descents. The solid curve along AB in Fig. 2 displays the path of the air touching the summit of the Puy de Dôme.

On 17 February, the flow was much simpler. As the inflow was from the west the air lived its first ascent when arriving at the Puy de Dôme. Its path is indicated in Fig. 2 by the solid line along C and D.

As both trajectories represent almost straight lines we used a cut along the cross-sections AB and CD as indicated by the dashed lines in Fig. 2. The flow fields in these 2 cross-sections are displayed in Figs. 4a,b for the 2 dates considered. We also see there the height of the topography as well as the liquid water field marked by differently shaded areas. We notice immediately the more complex pattern on the 15 February due to the northerly flow direction. The long-dashed line in Figs. 4a,b gives the trajectory, which touches the summit of the Puy de Dôme. We see that on 15 February this trajectory has passed other orographic clouds before while on 17 February the cloud resembles a textbook orographic cloud on an almost bell-shaped mountain and the trajectory passes only the cloud capping the Puy de Dôme. The trajectories touching the summit originated in both cases from altitudes between 150 m to 200 m above ground (Figs. 4a,b). However, it would be incorrect to assume that only this air determines the cloud on the summit. Also, air from the surface following the orography while ascending, as well as air from all levels in between will contribute to the summit air.

In order to estimate the contribution of the air from different levels in the atmosphere to the cloudy air at the summit we have made a numerical experiment by launching inert tracers at different altitudes. These altitudes correspond to the different levels of the model and are summarised in Table 3. The positions of the launching columns for the 2 meteorological situations are also indicated in Fig. 2 by the crosses. These

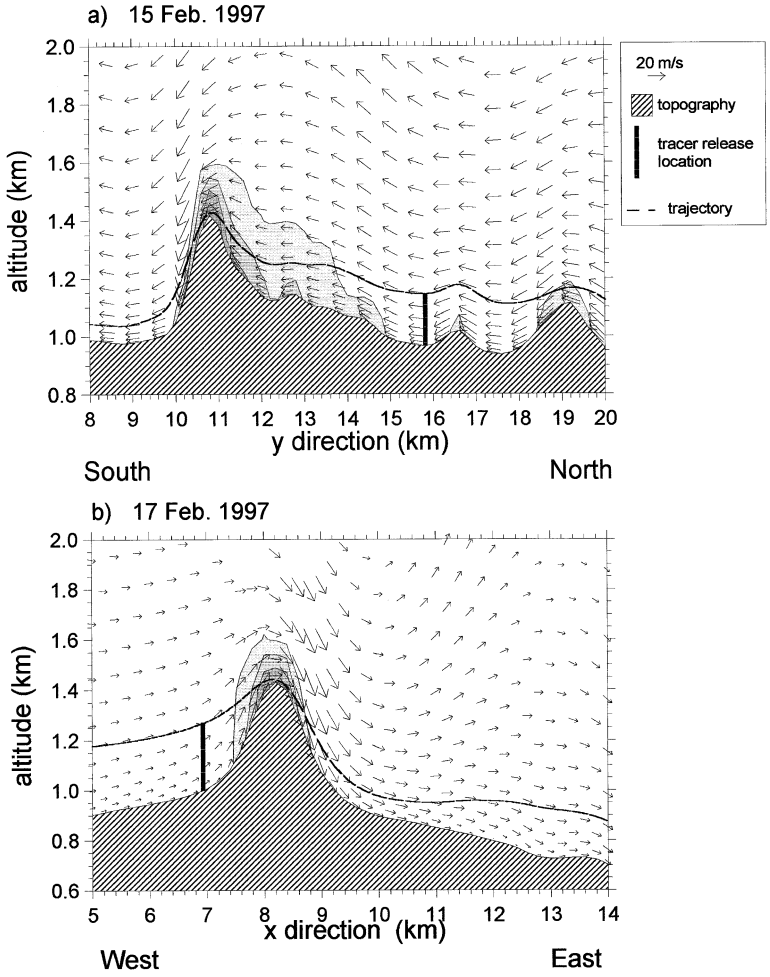

Fig. 4. Horizontal winds (m/s) and LWC (g/kg) as vertical cross-sections on (a) 15 February 1997 and (b) 17 February 1997, after 151 min of model time. The directions of the cross-section are indicated in Fig. 2 by AB(a) and CD (b). The 4 shaded areas for the LWC start at 0.03, 0.13, 0.23 and 0.33 g/m^3 and increase with darkening colour. The hatched area indicates the height of the topography. The columns give the position and height of the tracer releases and the dashed curve indicates the trajectory touching the summit (cf. Fig. 2).

positions were chosen about 1 km upwind of the modelled orographic cloud.

By launching an inert tracer in the 3-D model at different levels the diffusion of the tracer is followed and a certain concentration results at the summit. Superposing the results from the different launching levels allows calculating the relative contribution from each level in % to the total concentration level at the summit. These relative contributions are different for the 2 days considered and are summarised in Table 3. We see that for the 15 February the peak of the pollution mass results from levels near the surface. For 17 February, we notice a more balanced contribution from all altitudes considered with the maximum around 50 m above ground. This is due to the higher vertical wind shear producing a stronger mixing in the lower layers. Tracers launched at altitudes higher than the grazing trajectory were not found to contribute noticeably to the concentration at the summit. Concerning the influence of the position of the launching column we can

Table 3. *Atmospheric levels, corresponding altitudes (m) and percentage contribution of the tracer to the concentration at the summit for the 15 and 17 of February 1997*

No. model level	15/2/97 altitude (m)	15/2/97 % contribution (ε_i)	17/2/97 altitude (m)	17/2/97 % contribution (ε_i)
1	4	16	4	5.5
2	16	34.4	19	20.9
3	36	24.6	45	22.2
4	64	13.6	82	18.1
5	100	6.6	130	12.9
6	144	2.8	189	9
7	—	—	258	6

state that the absolute concentrations will be determined by the distance between the launching and the summit, however, the relative contribution of the different altitudes is insensitive as long as the column doesn't leave the traejctories indicated in Fig. 2.

In the following study the relative contributions from the different altitudes were used to weigh the results from parcel model calculations launched at the corresponding altitudes to obtain more realistic values for the microphysical properties calculated for the summit of the Puy de Dôme.

5.2. *Results of the microphysical models DESCAM and EXMIX*

5.2.1. Numerical studies of the droplet number density distribution function. The calculations of cloud microphysics with the models DESCAM and EXMIX were used to compare them with measurements of the drop number density distribution function and the scavenging fraction.

The results of the comparison of the drop number distribution are displayed in Figs. 5a,b for the 2 days considered. The measurements, representing 5 min means, are given by the fat curves and were taken by an FSSP situated outside the wind tunnel. In general, we notice that the measured droplet number concentrations are much lower than in other experiments on mountain sites in Europe (compare, e.g., the second and third GCE/EUROTRAC experiments on Kleiner Feldberg, Germany or Great Dun Fell, England; Arends et al., 1994; Hallberg et al., 1997). This could be expected already from the low number of aerosol particles and, thus, cloud condensation nuclei (compare Fig. 1). Obviously, the Puy de Dôme was exposed to rather clean air masses during the CIME 97 campaign.

Fig. 5a displays the results for 15 February. The solid and the dashed line give the results of the FSSP measurements for the droplet spectrum at 10:00 and 11:00. The 2 curves differ significantly from each other as during the observational period cold dry air was advected to the site and the cloud dissipated around noon time. At 11:00, the dissipation processes obviously has started already as the mean droplet diameter has dropped from 20 μm to 10 μm. This indicates that the cold dry air was probably mixed *homogeneously* with the cloudy air as a heterogenous mixing would have resulted rather in a constant diameter and a reduction in the number concentration of drops (Baker and Latham, 1979, 1982; Arends et al., 1994). However, as the number concentration in our measurements between 10:00 and 11:00 did not stay constant we cannot complete rule out the presence of heterogenous mixing. Unfortunately, the measurements at 10:00 and 11:00 were the only reliable observations of the drop spectrum during that day as the supercooled air rapidly iced the FSSP. Only directly after de-icing at 10:00 and 11:00 the measurements can be considered as free of artefacts. Nevertheless, we take the evolution of the droplet spectrum in the early dissipating stage of the cloud as an indicator for a dominating homogeneous mixing, justifying our model approach (see Subsection 3.4).

The results of the different models are displayed by the curves with the symbols. For the chemical composition of the particles we used the case A1 detailed in Table 4. We see here 3 different results produced by different applications of the DESCAM model and one result obtained with the EXMIX model. The solid triangles give the droplet distribution resulting from a cloud parcel ascending the mountain slope along the surface trajectory. The information gained from the mixing of an ensemble of trajectories with the coefficients detailed in Table 3 and Fig. 5 are given by the open diamonds for the case of no entrainment and by the full bullets for the case with entrainment. We see here that considering the entrainment process allows the droplet spectrum to broaden at the small size end as continuously

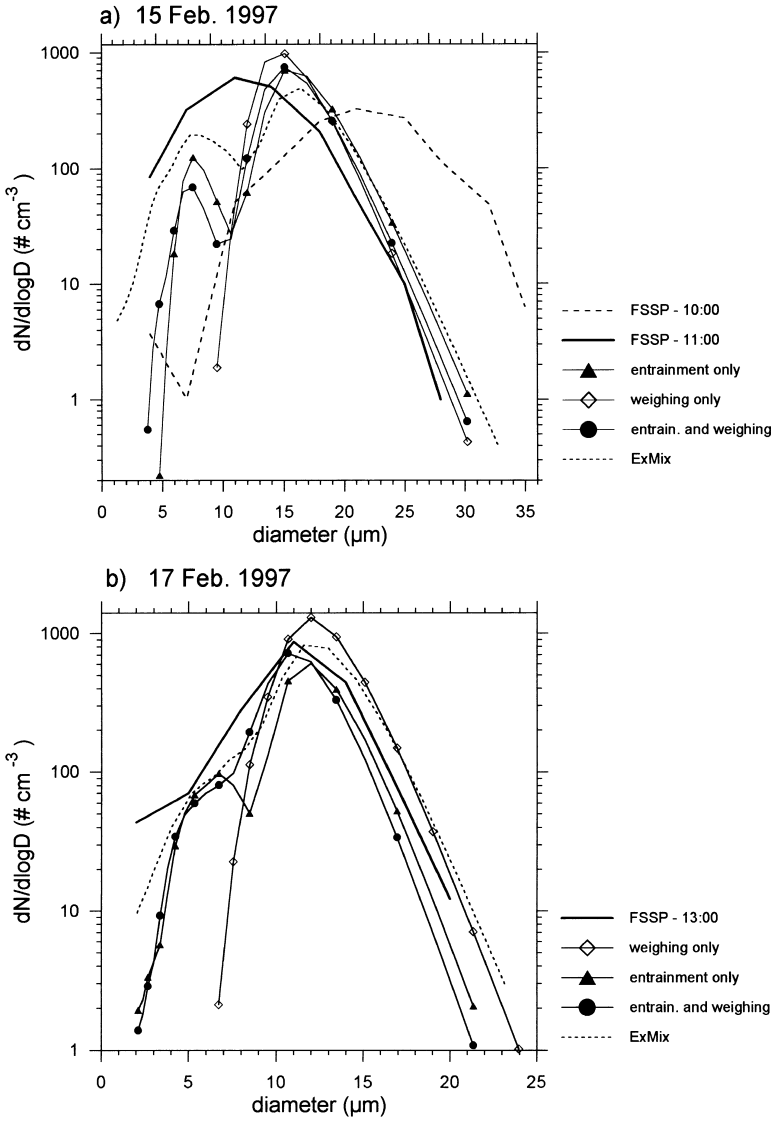

Fig. 5. Measured and calculated droplet spectra for 15 February 1997 (a) and 17 February 1997 (b). The solid lines represent the observations, the curves with the symbols pertain to different simulations as detailed in the text.

fresh nuclei are entrained forming new small droplets. Considering the mixing of an ensemble of trajectories adds to the broadening of the spectrum at the small end. The EXMIX model considering entrainment and weighing better fills the small end of the drop size distribution but also produces larger drops than DESCAM due to the different treatment of the supersaturation calculation. This results in the fact that the supersaturation of EXMIX exceeds the one of DESCAM by about a factor of 1.25. Still, a comparison with the observed spectrum is difficult due to the already mentioned heterogeneity of the cloud field.

This comparison is easier for 17 February (Fig. 5b) due to the simpler dynamic situation. Furthermore, no icing problems occurred due to the higher temperatures. Thus, the observed droplet spectrum remained almost constant for the

Table 4. *Summary of the cases with internally mixed aerosol particles considered for EXMIX; the first 4 parameters characterize the initial aerosol particle spectrum; S_{max} gives the modelled maximal supersaturation directly at cloud base; this results in an activation ("cut-off") diameter given in the last column*

Case	Chemical composition of the soluble part	Fraction of soluble material (ε)	Condensation coefficient α	Modification of the number of initial aerosol particles	S_{max} (%)	"cut-off" diameter (nm)
A1	$(NH_4)_2SO_4$	0.5	0.04		1.30	32
A2	$(NH_4)_2SO_4$	0.99	0.04		1.21	25
A3	$(NH_4)_2SO_4$	0.04	0.04		1.67	57
A4	NaCl	0.5	0.04		1.21	25
A5	$(NH_4)_2SO_4$	0.5	0.04	double number in each category	1.09	36
A6	$(NH_4)_2SO_4$	0.5	0.04	double number in sizes >100 nm	1.14	36
A7	$(NH_4)_2SO_4$	0.5	1.00		0.68	45
A8	$(NH_4)_2SO_4$	0.5	0.01		2.53	20

entire period considered. We see in Fig. 5b the same kind of information as in Fig. 5a (composition of particles according to case A1) and a comparison between the full triangles for the surface trajectory and the full bullets for the weighted ensemble trajectories shows that the weighing almost perfectly reproduced the location and strength of the maximum and improved the slope of the curve between 5 and 10 μm diameter. The agreement at the small sizes in both cases is still not satisfactory. Maybe entrainment and mixing is still too weak. The last curve to be found in Fig. 5b shows the result of the EXMIX model considering entrainment and weighing. Similar to the previous case we find that EXMIX reproduces better the small size range of the droplet spectrum below 10 μm diameter. However, it produces larger drops than the observations indicated, again due to the slightly higher supersaturations mentioned above.

In general, we can conclude that using the weighing of the different trajectories improves the results obtained with both microphysics models.

5.2.2. Numerical studies of the scavenging fraction. Another measured information to check the model performance against is the scavenging fraction as defined in eq. (1). For this study we have exclusively used the EXMIX model as its multi-dimensional number density distribution function allows a detailed sensitivity study of the scavenging fraction varying, e.g., the chemistry of the initial aerosol particle spectrum. Here, we have tried to reproduce the measurements as closely as possible. As the EXMIX model gives an information on the number density in each class we have used as separation between particles and drops the 5μm diameter as imposed by CVI and RJI. All categories are weighted with the efficiency curve of the CVI and the RJI yielding 50% at 5 μm (see Schwarzenböck (1998)). These numbers are counted as $N_{i,\mathrm{CVI}}$ or $N_{i,\mathrm{RJI}}$, respectively (compare eq. (1)).

The sensitivity studies performed are subdivided below into 2 different sections. In the first we will exclusively study the dependency of the scavenging fraction on the physical and chemical properties of the aerosol particles. In the second section we will consider the influence of the dynamics.

(a) *Sensitivity studies concerning the number density and chemical composition of the aerosol particles*

The Köhler equation (Pruppacher and Klett, 1997) allows to calculate the critical radius determining which aerosol particles are activated to form drops and which particles remain unactivated interstitial aerosol particles, thus determining the scavenging fraction. As parameters in the Köhler equation appear, among other quantities, the type of salt the particles are composed off, the solubility fraction ε, and the condensation coefficient α. Our first sensitivity test will be concerned

with these parameters (Table 4). As during 15 February more small Aitken-mode particles were activated it seems interesting to study the scavenging fraction during that day in more detail. At the end we will also discuss shortly the 17 February which represents the more classical situation of the stable cap cloud emerging the summit of the Puy de Dôme.

For 15 February, we chose from the different trajectories possible (see Subsection 5.1 and Table 3) the one originating at 144 m, corresponding to the situation in the upper part of the cloud affected by the mixing processes. As a reference for the tests concerning the scavenging fraction will serve case A1 where all particles are internally mixed with 50% $(NH_4)_2SO_4$ and 50% insoluble material like silicates. The condensation coefficient is assumed to 0.04 (Pruppacher and Klett, 1997). For the meteorological conditions studied this results in the formation of a cloud with a maximum supersaturation at cloud base of 1.3%. The Köhler equation then calculates a critical diameter, which corresponds to the class around 32 nm for activation. As all particles are alike in their chemical composition they behave in the same manner and this results in a steep "cut-off" in the scavenging fraction as illustrated in Fig. 6.

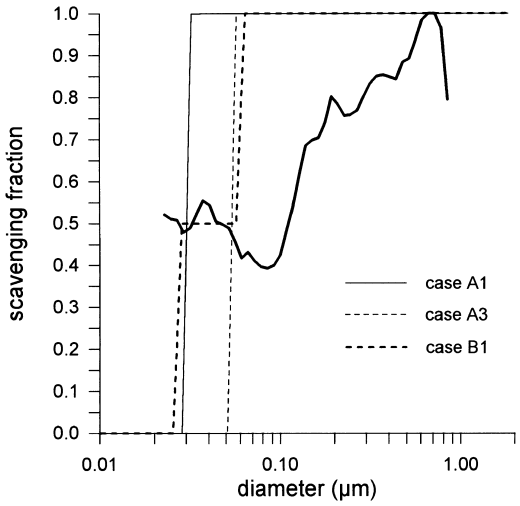

Fig. 6. Scavenging fraction as a function of dry aerosol particle diameter. The fat solid curve gives the measurements from 15 February at 11:00 LT. The fine curves pertain to cases A1, A3 and B1 (Tables 4 and 5) obtained for the simulation of 15 February 1997 with the trajectory originating as 144 m.

This steep slope persists for the other sensitivity studies summarised in Table 4. Only the position changes as a function of the solubility (e.g., more soluble particles activate more easily reducing the supersaturation and the "cut-off" diameter; case A2 and A3 (see Fig. 6)) and the type of salt (NaCl has a lower molecular weight than $(NH_4)_2SO_4$ thus reducing the supersaturation and the "cut-off" diameter; case A4). A further sensitivity study has been effected considering the number of aerosol particles. In case A5 we have doubled the number of particles in each category and in case A6 just the particles larger 100 nm were affected. The effect was very similar. The maximum supersaturation decreased with respect to the reference case A1 as more particles are activated. The reduced supersaturation increases the "cut-off" diameter to 36 nm. The "cut-off" diameter classes of case A5 and A6 are identical as the effect of the increased number of small particles in case A5 does not effect the supersaturation significantly (1.09 compared to 1.14). The last 2 tests of case A7 and A8 concern the condensation coefficient α. Here, we note that the variation between $\alpha = 1$ and $\alpha = 0.01$ has the largest impact on the "cut-off" or activation diameter in Table 4. Condensation coefficients covering this entire range have been reported in the literature (for a review see Pruppacher and Klett, 1997) where it is generally accepted that $\alpha = 1$ for pure water. With varying impurities lower condensation coefficients are found. A small condensation coefficient results in a reduced condensation causing a time lag with respect to the higher condensation coefficient. In the cases considered, $\alpha = 0.01$ took twice as long to reach the maximum supersaturation as $\alpha = 1$.

Svenningsson et al. (1992) have reported, e.g., that their growth studies during the GCE (Ground based Cloud) experiment of EUROTRAC have indicated that the aerosol population is not uniform. They have almost always found 2 different reservoirs, one with more hygroscopic particles ($\varepsilon \sim 0.4$–0.6) and another with less hygroscopic particles ($\varepsilon \sim 0.04$). During the second GCE experiment on the Kleiner Feldberg (Svenningsson et al., 1994) the reservoir of the less hygroscopic particles dominated over all size bins the more hygroscopic particles and contributed between 70–80% of the number concentration. During the 3rd GCE experiment of the Great Dun Fell

Table 5. *Summary of the cases with externally mixed aerosol particles considered for EXMIX; the first 6 parameters characterise the initial aerosol particle spectrum; S_{max} gives the modelled maximal supersaturation directly at cloud base; this results in one or more activation ("cut-off") diameters given in the last column*

	1st part			2nd part				
Case	% of particle number	fraction of $(NH_4)_2SO_4$ (ε)	condensation coefficient α	% of particle number	fraction of $(NH_4)_2SO_4$ (ε)	condensation coefficient α	S_{max} (%)	"cut-off" diameter (nm)
B1	50	0.5	0.04	50	0.04	0.04	1.45	64/28
B2	80	0.5	0.04	20	0.04	0.04	1.34	72/32
B3	20	0.5	0.04	80	0.04	0.04	1.57	64/28
B4	50	1.0	1.0	50	0.04	0.02	1.14	72/28
B5	100 of $D > 100$ nm 0 else	0.5	0.04	100 of $D < 100$ nm 0 else	0.04	0.04	1.6	64
B6	100 of $D > 100$ nm 0 else	0.04	0.04	100 of $D < 100$ nm 0 else	0.5	0.04	1.35	32

(Svenningsson et al., 1997), however, the less hygroscopic particles only contributed 10–20% to the total number concentration. Consequently, our second set of sensitivity tests (Table 5) analyses the impact of the different percentages of less soluble and more soluble particles on the scavenging ratio. Case B1 which is also displayed in Fig. 6 investigates the scavenging ratio of an aerosol particle population where 50% of the number are more hygroscopic ($\varepsilon = 0.5$) and 50% are less hygroscopic ($\varepsilon = 0.04$). We see here that in contrast to the internally mixed aerosol the externally mixed aerosol produces steps in the scavenging ratio. The first one at 28 nm is due to the complete activation of the more hygroscopic particles and the second one at 64 nm pertains to the less hygroscopic ones, which activate less easily. Changing the number contribution of the more and less hygroscopic particles as done in case B2 and B3 affects the size and the position of the steps. Different values for the condensation coefficient have a further influence on the steps (case B4). For last tests of this series we applied the separation between more and less hygroscopic particles not uniformly over the entire particle spectrum but attributed one solubility to the small particles and another to the large particles (cases B5 and B6). The result resembles again at curve A1 or A3 in Fig. 6 as just one "cut-off" is created. The step disappears as the number density and the composition of the small particles ($D <$ 100 nm) dominates the behaviour of the scavenging fraction.

The sensitivity studies summarise the variability of the scavenging fraction with respect to the physical and chemical properties of the aerosol particles. Certainly, it would have been possible to approach more closely the observed curves in considering more explicitly the heterogeneity in size and solubility of the chemical composition in natural aerosol particles and in taking into account co-condensation of other soluble gases as proposed, e.g., in Kulmala et al. (1996) and Laaksonen et al. (1998). Given the uncertainties in the necessary assumptions concerning the composition of the aerosol particles and the concentration of simultaneously present trace gases we will, however, terminate the study of the physico-chemistry of the aerosol particles at this point. Also, considering the shape of the measured scavenging ratio we have to admit that also other factors might intervene to explain the observed curves (compare, e.g., Fig. 6). Consequently, below we will study the sensitivity of the scavenging ratio concerning dynamical aspects.

(b) *Sensitivity studies concerning the dynamics*

In part (a) the evolution of the aerosol particle spectrum was studied in a closed rising air parcel.

Table 6. *Summary of the cases with homogeneous entrainment considered for EXMIX; the first 4 parameters characterise the initial aerosol particle spectrum; S_{max} gives the modelled maximal supersaturation directly at cloud base; this results in an activation ("cut-off") diameter given in the last column*

	1st part		2nd part			
Case	% of particle number	fraction of $(NH_4)_2SO_4$ (ε)	% of particle number	fraction of $(NH_4)_2SO_4$ (ε)	S_{max} (%)	"cut-off" diameter (nm)
C1	100	0.5	—	—	1.30	32
C2	50	0.5	50	0.04	1.45	28
C3	50	0.02	50	0.7	1.44	25
C4	20	0.02	80	0.7	1.32	28
C5	80	0.02	20	0.7	1.61	25

We know, however, that air parcels moving in the atmosphere are not completely closed but exchange mass and energy with the environment via entrainment. As detailed in Section 3 the entrainment for an individual air parcel was assumed as being homogeneous which is a rather simplified approach. Still, the replenishment of aerosol particles via entrainment of particles from the environment helps to smooth the steep steps produced by the cases A and B. The considered cases are summarised in Table 6 and partly displayed in Fig. 7. As entrainment smears out the curves we will just give the lowest "cut-off" diameter in Table 6. Case C1 represents case A1 (internally mixed aerosol particles) but with considering entrainment processes. We find that the maximum supersaturation and the "cut-off" diameter are the same as from case A1 as these are determined close to cloud base. Entrainment acts during the entire ascent of the parcel while the supersaturation drops again. The newly entrained particles cannot activate any more and already activated particles are detrained. This tends to smear out the curve and is especially responsible for the fact that the curve does not reach 100% any more for larger diameters (compare Fig. 7). This behaviour is confirmed by case C2 that represents case B1 with inclusion of entrainment. The steps, which appear in Fig. 6, are barely recognisable in Fig. 7. Also, the tests C3 to C5 show that the entrainment together with the external mixture in the composition of the aerosol particles can explain occasional plateaux in the scavenging fraction (Fig. 7).

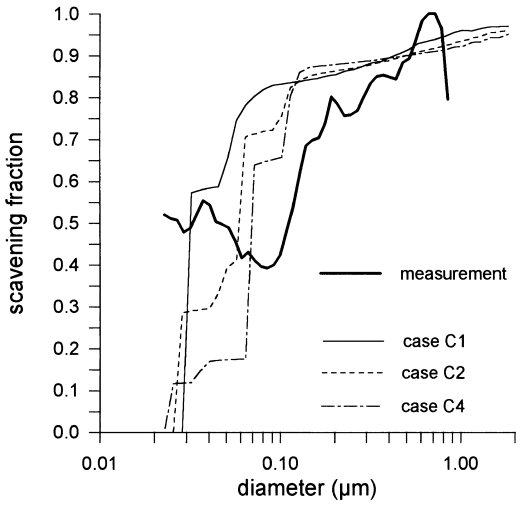

Fig. 7. Scavenging fraction as a function of dry aerosol particle diameter. The fat solid curve gives the measurements from 15 February at 11:00 LT. The thin curves represent the results from the cases C1, C2 and C4 as detailed in Table 6 considering homogeneous entrainment.

The results so far were all obtained using a single trajectory originating at 144 m above ground. From Subsection 5.1 it is clear that air from different levels reach the summit of the Puy de Dôme following different trajectories.

Thus, in a last set of tests we applied the weighing functions derived in Subsection 5.1. The cases B1 (external mixture, no entrainment) and C2 (external mixture, with entrainment) considering the weighing function are displayed in Fig. 8. Comparing with Fig. 7 we see that by introducing the weighing function, the scavenging ratio is smoothed again resembling more case B1 (Fig. 6). This is due to the fact that the scavenging

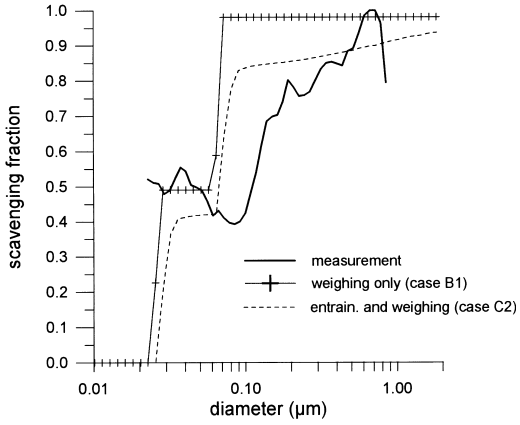

Fig. 8. Scavenging fraction as a function of dry aerosol particle diameter. The fat solid curve gives the measurements from 15 February at 11:00 LT. The thin curves represent the results from the cases B1 and C2 as detailed in Tables 5, 6 considering entrainment with the weighting factors given in Fig. 5 and Table 2.

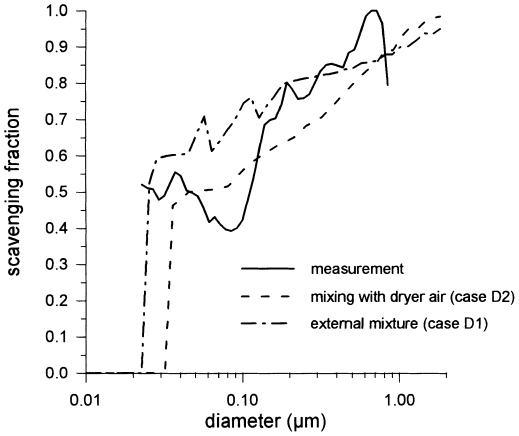

Fig. 9. Scavenging fraction as a function of dry aerosol particle diameter. The fat solid curve gives the measurements from 15 February at 11:00 LT. The thin curves represent the results from cases D1 and D2 as detailed in the text.

ratio now is a mixture of different air parcels. Thus, only the essential step is retained. The other plateaux introduced by the entrainment are smoothed out by the mixture of 6 different trajectories.

Comparing the sensitivity tests with the measured curves of the scavenging fraction we can conclude that we are still not able to successfully reproduce its shape. We are lacking essential elements like the size dependent composition of the particles and the exact type of mixing active during the cloud event. We can, however, arbitrarily play with the open parameters of the problem. Fig. 9 displays 2 simulations where we tested again the effect of entrainment and mixing onto the scavenging fraction. One curve in Fig. 9 pertains to a mixture with 3 different types of particles which are internally and externally mixed (case D1: $D < 60$ nm, $\varepsilon = 0.5$; 60 nm $< D <$ 120 nm, $\varepsilon = 0.28$; $D > 120$ nm, $\varepsilon = 0.04$; salt: $(NH_4)_2SO_4$) and are exposed to a homogeneous entrainment. We see that then even local maxima and minima occur. In the second curve we have artificially modified the entrainment by tripling the entrainment in the last 100 m below the summit (case D2: same aerosol composition as case C2). This was done by increasing the dewpoint difference with the environment to 1°C (before 0.2°C) to mimic an increased entrainment near cloud top. Comparing these curves qualitatively to the observed scavenging fractions we find a closer agreement.

Fig. 10 displays the situation for 17 February. Here, we selected the trajectory originating at 130 m and varied the composition of the particles. For case E1, 50% of the particles were less soluble $\varepsilon = 0.04$ and 50% more soluble $\varepsilon = 0.5$ and a homogeneous entrainment was considered. For case E2, 70% of the particles were assumed to be

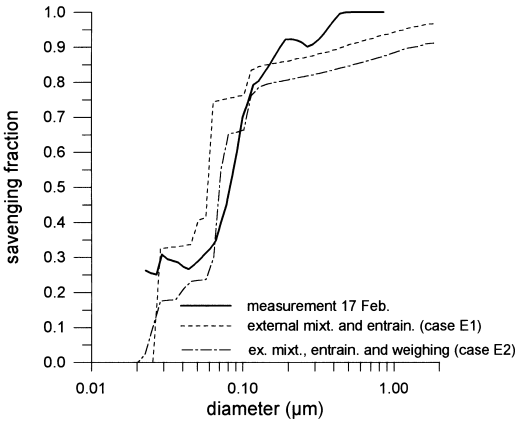

Fig. 10. Scavenging fraction as a function of dry aerosol particle diameter. The fat solid curve gives the measurements from 17 February at 13:00 LT. The thin curves represent the results from cases E1 and E2 as detailed in the text.

less soluble $\varepsilon = 0.04$ and 30% were almost totally soluble $\varepsilon = 0.9$. Here, entrainment and weighing of the trajectory ensemble were considered. We see that case E2 reproduces rather well the step in the scavenging fraction. We can state that it is much easier to reproduce the measurements for 17 February than for 15 February. This is caused by the much simpler dynamical situation prevailing as already detailed above.

Thus, we can conclude from the cases studied that it will be possible to reach agreement between experiment and models, but as too many free parameters exit at the moment we cannot quantify the contribution of each factor studied to the observed scavenging fraction. The situation is a bit easier in simple dynamical situations (orographic clouds), however, more difficult in complex geographic situations and frontal systems.

6. Summary and conclusions

During February 1997 one of the 2 observational periods of CIME (*c*loud *i*ce *m*ountain *e*xperiment), a joint field experiment funded by the European Commission in order to study the fate of pollutants during the freezing of a cloud, took place on the summit of the Puy de Dôme in the centre of France. During this experiment the droplet spectra were measured with an FSSP and the aerosol particles in the drops and in the interstitial particle phase were measured with a counterflow virtual impactor and by means of a round jet impactor inside a windtunnel, respectively. For the first time here the activation of small Aitken-mode particles, as low as 25 nm were observed.

Two datasets obtained on 15 February and 17 February were used to compare them to detailed model calculations in order to try to understand the activation of the particles and the spectral form of the droplet spectrum and the scavenging fraction.

In order to account for the mixing processes inside the cloud which are likely to have an important influence on the microphysical and chemical properties of the cloud we used a new approach. We have considered that the air at the summit of a mountain is a composite of air climbing the slope of the mountain and air that is transported along elevated trajectories. In order to have a correct representation of the percentages of air coming from the different altitudes we have launched tracers at 6 different levels in a 3-dimensional mesoscale model. Their relative contribution to the summit air allowed to derive a weighing function.

In order to calculate the microphysical and scavenging properties at the summit we have launched 6 air parcels originating at these 6 different altitudes upwind of the summit. The trajectories ended all at the summit and the weighing function allows to calculate an average value to be compared to the observations.

As parcel models we have used the DESCAM and the EXMIX model. The DESCAM model is a spectral model which has been used in past already coupled to a 2-D dynamical model (e.g., Flossmann, 1994) and represents a compromise in accuracy and efficiency for calculating detailed microphysics and scavenging properties of clouds. In addition, it contains all microphysical process up to the formation of raindrops. It was used to compare it with the FSSP measurements. The EXMIX model allows to calculate the microphysics and scavenging properties of a cloud in even more details as it follows drops and aerosol particles in a multi-dimensional distribution function. Thus, it is very suitable to mimick the detailed measurements with CVI and RJI as taken during CIME.

Using the 2 detailed models embedded in the trajectory calculated by the 3-D model we arrive at the following conclusions.

Using a homogeneous entrainment approach for the air parcel models allows to reproduce the observed *droplet spectra* reasonably well. The assumption of a homogeneous entrainment is also supported by the measurements. Both models notice an improvement in the simulations considering the derived weighing function.

Considering the *scavenging fraction* we notice a significant influence resulting from the chemical composition of the particles and the condensation coefficient. Also a large influence was found for the dynamical aspects, i.e., entrainment and mixing. Here, the effect of the weighing function was less convincing since the scavenging fraction is largely determined by the activation taking place directly at cloud base and to a lesser degree by the mixing processes. Concerning the activation of the small Aitken-mode particles we note that

our approach is able to predict activated particles as low as 25 nm diameter. The measurements, however, indicate with the fact that the scavenging fraction does not drop to zero at 25 nm that even smaller particles were activated. This is difficult to explain in view of the already high supersaturations obtained in the calculations. These supersaturations obtained in the model, however, appear realistic since the total number of particles measured was rather low. This low number concentration was identified to be the origin of the low activation radius. As the number concentrations measured, e.g., during the 2nd and the 3rd GCE/EUROTRAC campaign were a factor 3 to 10 higher than the actual number concentrations it becomes clear why such low activation radii have not been reported before.

In general, we can conclude that the variability found in the sensitivity tests allows to reproduce the shape of the observed results. As too many free parameters exit at the moment we cannot quantify the contribution of each factor studied to the observed scavenging fraction. However, a spectral knowledge of the chemistry of the particles, e.g., would certainly provide a promising basis to reproduce the measurements with less ambiguity. For the case of a simple dynamical situation the results are already almost satisfactory. For a more complex topography and advected dynamical systems like fronts more improvements are required. The models DESCAM and EXMIX perform both reasonably well to confirm the confidence in their application to other atmospheric situations.

7. Acknowledgements

The authors acknowledge with gratitude the support by the European Commission under ENV4-CT95-0012. They are solely responsible for the content of this manuscript. The calculations for this paper have been done on the CRAY C98 and C94 of the "Institut du Développement et des Ressources en Informatique Scientifique" (IDRIS, CNRS) in Orsay (France) under project no. 940180. The authors acknowledge with gratitude the hours of computer time and the support provided.

REFERENCES

Arends, B. G., Kos, G. P. A., Maser, R., Schell, D., Wobrock, W., Winkler, P., Ogren, J. A., Noone, K. J., Hallberg, A., Sveningsson, I. B., Wiedensohler, A., Hansson, H.-C., Berner, A., Sooly, I. and Kruisz, C. 1994. Microphysics of clouds at Kleiner Feldberg. *J. Atmos. Chem.* **19**, 59–86.

Baker, M. B. and Latham, J. 1979. The evolution of droplet spectra and rate of production of embryonic rain drops in small cumulus clouds. *J. Atmos. Sci.* **36**, 1612–1615.

Baker, M. B. and Latham, J. 1982. A diffusive model of the turbulent mixing of dry and cloudy air. *J. Atmos. Sci.* **108**, 871–898.

Baker, M. B., Corbin, R. G. and Latham, J. 1980. The influence of entrainment on the evolution of cloud droplet spectra (I). A model of inhomogeneous mixing. *Q. J. R. Meteorol. Soc.* **106**, 581–598.

Bruintjes, R. T., Clark, T. L. and Hall, W. D. 1995. The dispersion of tracer plumes in mountainous regios in Central Arizona. Comparison between observations and modelling results. *J. Appl. Met.* **34**, 971–988.

CIME, 1998. *Cloud ice mountain experiment final report* (ed. Flossmann, A.). European Commission; ENV4-CT95-0012 (DG12-DTEE), available from the EC.

Clark, T. L. 1977. A small scale dynamic model using terrain-following coordinate transformation. *J. Comput. Phys.* **24**, 186–215.

Clark, T. L. 1979. Numerical simulations with a three dimensional cloud model. *J. Atmos. Sci.* **36**, 2191–2215.

Clark T. L. and Gall, R. 1982. Three dimensional numerical model simulations of air flow over mountainous terrain. A comparison with observation. *Mon. Wea. Rev.* **110**, 766–791.

Clark, T. L and Farley, R. D. 1984. Severe downslope windstorm calculations in two and three spatial dimensions using anelastic interactive grid nesting. *J. Atmos. Sci.* **41**, 329–350.

Clark, T. L., Hall, W. D. and Banta, R. M. 1994. Two and three dimensional simulations of the 9 Jan 1989 severe Boulder windstorm: comparison with observation. *J. Atmos. Sci.* **51**, 2317–2342.

Colvile, R. N., Sander, R., Choularton, T. W., Bower, K. N., Inglis, D. W., Wobrock, W., Schell, D., Svenningsson, I. B., Wiedersohler, A., Hansson, H.-C., Hallberg, A., Ogren, J. A., Noone, K. J., Facchini, M. C., Fuzzi, S., Orsi, G., Arends, B. G., Winniwarter, W., Schneider, T. and Berner, A. 1994. Computer modelling of clouds at Kleiner Feldberg. *J. Atmos. Chem.* **19**, 189–229.

Flossmann, A. I. 1991. The scavenging of two different types of marine aerosol particles using a two-dimensional detailed cloud model. *Tellus* **43B**, 301–321.

Flossmann, A. I. 1994. A 2-D spectral model simulation of the scavenging of gaseous and particulate sulfate by a warm marine cloud. *J. Atmos. Res.* **32**, 255–268.

Flossmann, A. I. and Pruppacher, H. R. 1988. A theoretical study of the wet removal of atmospheric pollutants. Part III. *J. Atmos. Sci.* **45**, 1857–1871.

Flossmann, A. I., Hall, W. D. and Pruppacher, H. R. 1985. A theoretical study of the wet removal of atmospheric pollutants. Part I. *J. Atmos. Sci.* **42**, 582–606.

Flossmann, A. I., Pruppacher, H. R. and Topalian, J. H. 1987. A theoretical study of the wet removal of atmospheric pollutants. Part II. *J. Atmos. Sci.* **44**, 2912–2923.

Hall, W. D. 1980. A detailed microphysical model within a two-dimensional dynamic framework: model description and preliminary results. *J. Atmos. Res.* **37**, 2486–2507.

Hallberg, A., Ogren, J. A., Noone, K. J., Okada, K., Heintzenberg, J. and Sveningsson, I. B. 1994. The influence of aerosol particle composition on cloud droplet formation. *J. Atmos. Chem.* **19**, 153–171.

Hallberg, A., Wobrock, W., Flossmann, A. I., Bower, K. N., Noone, K. J., Wiedensohler, A., Hansson, H.-C., Wendisch, M., Berner, A., Kruisz, C., Laj, P., Facchini, M. C., Fuzzi, S. and Arends, B. G. 1997. Microphysics of clouds: models vs. measurements. *Atmos. Environ.* **16**, 2453–2462.

Hatzianastassiou, N., Wobrock, W. and Flossmann, A. I. 1998. The effect of cloud-processing of aerosol particles on clouds and radiation. *Tellus* **50B**, 478–490.

IPCC. 1995. *Climate change 1995. The science of climate change* (eds. Houghton, J. T., Meira Filho, L. G., Callander, B. A., Harris, N., Kattenberg, A. and Maskell, K). Cambridge University Press.

Jaenicke, R. 1988. Aerosol physics and chemistry. In: Landolt-Boernstein: *Zahlenwerte und Funktionen aus Naturwissenschaften und Technick*, V **4b**. G. Fischer, ed. Berlin: Springer, 391–457.

Kulmala, M, Korhonen, P., Vesala, T., Hansson, H.-C., Noone, K. and Svenningsson, B. 1996. The effect of hydroscopicity on cloud formation. *Tellus* **48B**, 347–360.

Laaksonen, A., Korhonen, P., Kulmala, M. and Charlson, R. J. 1998. Modification of the Kohler Equation to include soluble trace gases and slightly soluble substances. *J. Atmos. Sci.* **55**, 853–862.

Laj, P., Fuzzi, S., Facchini, M. C., Orsi, G., Berner, A., Kruisz, C., Wobrock, W., Hallberg, A., Bower, K. N., Gallagher, M. W., Beswick, K. M., Colvile, R. N., Choularton, T. W., Nason, P. and Jones, B. 1997. Experimental evidence for in-cloud production of aerosol sulphate. *Atmos. Environ.* **31**, 2503–2514.

Martinsson, B. G., Cederfelt, S. I., Svenningsson, B., Frank, G., Hansson, H.-C., Swietlicki, E. and Wiedensohler, A. 1997. Experimental determination of the connection between cloud droplet size and its dry residue size. *Atmos. Environ.* **31**, 2490–2499.

Noone, K. J., Ogren, J. A., Hallberg, A., Heintzenberg, J., Ström, J., Hansson, H.-C., Svenningsson, B., Wiedensohler, A., Fuzzi, S., Facchini, M. C. and Berner, A. 1992. Changes in aerosol size and phase distribution due to physical and chemical processes in fog. *Tellus* **44B**, 489–504.

Ogren, J. A., Heintzenberg, J. and Charlson, R. 1985. In situ sampling of clouds with a droplet to aerosol converter. *Geophys. Res. Lett.* **12**, 121–123.

Pruppacher, H. R. and Klett, J. D. 1997. *Microphysics of clouds and precipitation.* Kluwer Academic Publishers, 2nd revised and enlarged edition. 954 pp.

Schell, D., Wobrock, W., Maser, R., Preiss, M., Jaeschke, W., Georgii, H.-W., Gallagher, M. W., Bower, K. N., Beswick, K. M., Pahl, S., Facchini, M. C., Fuzzi, S.. Wiedensohler, A., Hansson, H.-C. and Wendisch, M. 1997. The size-dependent chemical composition of cloud droplets. *Atmos. Environ.* **31**, 2561–2576.

Schwarzenböck, A., Heintzenberg, J. and Mertes, S. 1999. New minimum lower cut size for a counterflow virtual impactor complemented by the upper cut of an interstitial inlet. *J. Aerosol Sci.* **28**, 277–278.

Schwarzenböck, A. 1998. *Development and application of complementary hydrometeor and interstitial aerosol samplers.* PhD thesis. available from University of Leipzig, Germany.

Schwarzenböck, A., Heintzenberg, J., Mertes, S. and Wiedensohler, A. 1998. Correlations of the partitioning fraction in clouds. *J. Aerosol Sci.* **29**, 53–54.

Svenningsson, B., Hansson, H.-C., Wiedensohler, A., Ogren, J. A., Noone, K. J. and Hallberg, A. 1992. Hygroscopic growth of aerosl particles in the Po Valley. *Tellus* **44B**, 556–569.

Svenningsson, B., Hansson, H.-C., Wiedensohler, A., Noone, K. J., Ogren, J. A., Hallberg, A. and Colvile, R. 1994. Hygroscopic growth of aerosol particles and its influence on nucleation scavenging in clouds: experimental results from Kleiner Feldberg. *J. Atmos. Chem.* **19**, 129–152.

Svenningsson, B., Hansson, H.-C., Martinsson, B., Wiedensohler, A., Swietlicki, E., Cederfelt, S.-I., Wendisch, M., Bower, K. N., Choularton, T. W. and Colvile, R. N. 1997. Cloud droplet nucleation scavenging in relation to the size and hygroscopic behaviour of aerosol particles. *Atmos. Environ.* **31**, 2463–2476.

Twomey, S. 1959. The nuclei of natural cloud formation. Part II: The supersaturation in natural clouds and the variation of cloud droplet concentration. *Geophys. Pura a Applicata* **43**, 243–249.

Warner, J. 1969. The microstructure of cumulus clouds: Part II: The effect on drop size distribution of cloud nucleus spectrum and updraft velocity. *J. Atmos. Sci.* **26**, 1272–1282.

Warner, J. 1973. The microstructure of cumulus clouds. Part IV: The effect on the droplet spectrum of mixing between cloud and environment. *J. Atmos. Sci.* **30**, 256–261.

Wobrock, W. 1986. *Numerische Modellsimulationen von Strahlungsnebelepisoden unter Berücksichtigung spektraler Wolkenmikrophysik.* PhD Thesis, available

from Johannes-Gutenberg Universität, Frankfurt, Germany.

Wobrock, W., Schell, D., Maser, R., Jaeschke, W., Georgii, H.-W., Wieprecht, W., Arends, B. G., Mols, J. J., Kos, G. P. A., Fuzzi, S., Facchini, M. C., Orsi, G., Berner, A., Solly, I., Kruisz, C., Svenningsson, I. B., Wiedensohler, A., Hansson, H.-C., Ogren, J. A., Noone, K. J., Hallberg, A., Phal, S., Schneider, T., Winkler, P., Winiwarter, W., Colvile, R. N., Choularton, T. W., Flossmann, A. I. and Borrmann, S. 1994. The Kleiner Feldberg Cloud Experiment, 1990. An Overview. *J. Atmos. Chem.* **19**, 3–35.

Wobrock, W., Flossmann, A. I., Colvile, R. N. and Inglis, D. W. F. 1997. Modelling of airflow and cloud fields over the northern Pennines. *Atmos. Environ.* **31**, 2421–2439.